

Temperature dependent thermal conductivity increase of aqueous nanofluid with single walled carbon nanotube inclusions

Sivasankaran Harish¹, Kei Ishikawa¹, Erik Einarsson^{1,2}, Shinya Aikawa¹, Taiki Inoue¹,
Pei Zhao¹, Makoto Watanabe¹, Shohei Chiashi¹, Junichiro Shiomi¹, Shigeo Maruyama^{1*}

¹Department of Mechanical Engineering, The University of Tokyo, 7-3-1 Hongo, Bunkyo-ku,
Tokyo 113-8656, Japan

²Global Center of Excellence for Mechanical Systems Innovation, The University of Tokyo,
7-3-1 Hongo, Bunkyo-ku, Tokyo 113-8656, Japan

Abstract

We investigated the thermal and electrical conductivity of water seeded with single-walled carbon nanotubes (SWCNT) synthesized using the alcohol catalytic chemical vapour deposition method. Sodium deoxycholate was used as the surfactant to prepare stable nanofluids, which we then thoroughly characterized by microscopic and spectroscopic methods. Electrical conductivity measurements showed power law dependence with respect to SWCNT loading, while the thermal conductivity increase showed a linear dependence on loading. The effective thermal conductivity of the nanofluid was also found to increase with increasing temperature. Viscosity of the nanofluids showed a threefold increase compared to the thermal conductivity increase, which may play a crucial role in utilizing this fluid for practical applications. We compare experimental results with existing analytical models and discuss the critical role of thermal boundary resistance, which limits the improvement in thermal conductivity. Influence of SWCNT aggregation in the increase of effective thermal conductivity is also discussed.

1. Introduction

Technological advancements in the field of nanotechnology have led to the development of a new class of fluids termed “nanofluids”. Over the past decade, conventional heat transfer fluids seeded with nanomaterials have attracted thermal scientists because of the expected superior thermal properties of these nanofluids, and many research groups have reported significant improvements in conductive¹ and convective heat transfer² properties.

Nanomaterials are typically spherical or cylindrical in shape. Nanofluids consisting of spherical particles have used various metals and metallic oxides. These predominantly include copper, copper oxide, aluminum, aluminum oxide, zinc oxide, titanium dioxide, gold, silver etc.¹⁻³. The influence on thermal conductivity increment caused by seeding the above-mentioned spherical particles in different base fluids has been well summarized by several reports^{1,3,4}. Very high improvement in the thermal conductivity was reported with the inclusion of spherical particles by few reports⁵ while many research groups failed to observe such anomalous improvement⁴. A recent benchmark study found no such anomalous improvement with spherical nanoparticles but high improvement for the inclusion of cylindrical structures⁶.

The first experimental observation of thermal conductivity increase using cylindrical structures, namely multi-walled nanotubes (MWCNT), was reported by Choi and co-workers⁷. They reported a thermal conductivity increase of 160% for the case of MWCNTs dispersed in poly-(α olefin) oil at a nanotube loading of 1 vol%. The prime reason behind the selection of CNTs was due to their high thermal conductivity. Experimental and numerical studies have reported very high thermal conductivity for CNTs⁸⁻¹⁴. Hence, it is natural to expect that the suspensions consisting of CNTs would result in higher thermal conductivity increase compared to other nanoparticles. However, the anomalous increment reported by Choi et al⁷. could not be reproduced in subsequent studies¹⁵⁻²⁰. All the above-mentioned measurements were performed with MWCNTs and the number

of experiments with SWCNTs remains limited. We believe that a direct comparison of the experimental results cannot be made without the knowledge of all important parameters, such as the length of CNTs, number of walls, crystallinity of MWNTs, preparation method, purity level and pH of the fluid. Proper characterization of MWCNTs was not performed by many research groups and the nanofluid preparation technique was found to vary among groups. This could be a potential reason for the inconsistent data prevailing in the literature for CNT-based nanofluids. Therefore, to understand the real potential of nanofluids, we prepared SWCNT based nanofluids in water using sodium deoxycholate (DOC) as the surfactant commonly used for photoluminescence spectroscopy measurements which requires complete dispersion. We characterized the SWCNTs using transmission electron microscopy (TEM), resonance Raman spectroscopy, atomic force microscopy (AFM), optical absorption spectroscopy (OAS) and photoluminescence excitation spectroscopy (PLE). We performed thermal conductivity measurements using a transient hot wire technique, and also measured the effective electrical conductivity and viscosity of the SWCNT nanofluids. Here we compare our experimental results with classical analytical models and discuss the possible mechanism behind the thermal conductivity increase reported in this work.

2. Materials and methods

2.1 Synthesis of single-walled carbon nanotubes from alcohol

We synthesized SWCNTs by alcohol catalytic chemical vapour deposition (ACCVD) technique²¹. This technique employs cobalt and iron bi-metallic catalysts supported on a zeolite particle (HSZ-390HUA). It utilizes ethanol vapour as the carbon feedstock, and the reaction temperature was maintained at 800°C. After CVD synthesis zeolite particles were removed by dissolving in sodium hydride solution.

2.2 Raman and Transmission Electron Microscopy (TEM) characterization

The SWCNTs were analyzed using transmission electron microscopy (JEOL, JEM-2000EX) and resonance Raman spectroscopy. For TEM imaging, the samples were prepared by sonicating in ethanol for 30 minutes, after which 10 μl of the solution was dropped on a TEM microgrid and allowed to evaporate. A typical TEM image of the SWCNTs synthesized from ethanol feedstock is shown in Figure 1. The TEM image clearly shows that the SWCNTs were devoid of both amorphous carbon and metal nanoparticle impurities.



Figure 1: TEM image of SWCNTs synthesized from ethanol feedstock. Image captured at an acceleration voltage of 120 kV.

Raman spectra of the SWCNTs were acquired using a micro-Raman apparatus with a 50 cm single monochromator and a CCD detector (Chromex 501is with Andor DV401-F1). An argon ion laser with a wavelength of 488 nm (2.54 eV) and a Helium–Neon laser with a wavelength of 633 nm (1.96 eV) were used to obtain the spectra. A typical spectrum obtained from the SWCNT sample is shown in Figure 2. Two dominant

features noticed in RRS are the radial breathing mode (RBM) at low frequencies and the tangential multi-feature (G-band) at higher frequencies.

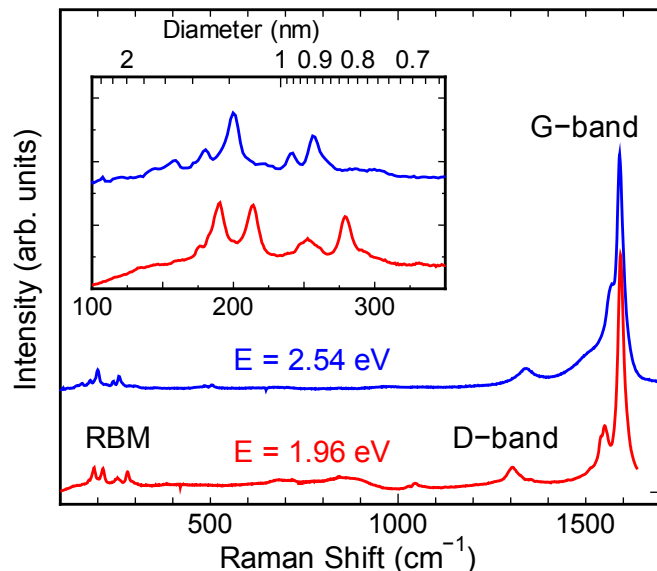


Figure 2: Resonance Raman spectra of ACCVD SWCNTs. The G-band, D-band and the radial breathing mode (RBM) peaks are shown. An expanded view of the RBM signals with an added diameter scale is shown in the inset.

RBM peaks seen in the low-frequency region ($100\text{--}400\text{ cm}^{-1}$) are unique to SWCNTs and are not observed in other carbon allotropes²². An interesting feature of the RBM is that the RBM frequency (ω_{RBM}) is proportional to the inverse of the nanotube diameter, following the equation $\omega_{\text{RBM}} = A/d_t + B$, where d_t (nm) is the diameter of the nanotube, and A ($\text{cm}^{-1}\text{ nm}$) and B (cm^{-1}) are empirical constants. For the present case, values of 217.8 and 15.7 are used for A and B respectively²³. The expanded RBM signal along with the diameter scale is shown in the inset of Figure 2. From the inset it can be seen that the sample contains SWCNTs with diameters ranging from 0.8-1.6 nm²¹.

The G-band observed at 1592 cm^{-1} is a characteristic feature of sp^2 -bonded graphitic carbon, and corresponds to in-plane vibrations of the carbon atoms. In addition to the G-band and RBM, a third feature found near 1350 cm^{-1} (the D-band) arises from defects in the tube walls or from amorphous carbon impurities. The relative intensity of the G-band with respect to the D-band (I_G/I_D) is representative of the crystallinity of the SWCNTs. In the as grown sample, a large I_G/I_D indicates good crystallinity of the SWCNTs. TEM investigation also clearly showed the absence of metal and amorphous carbon impurities, hence the SWCNTs do not require an additional purification process.

2.3 Nanofluid preparation

The highly hydrophobic nature of SWCNTs makes it very difficult to disperse them in water. An important prerequisite for a nanofluid is the preparation of a stable and homogenous dispersion. In our present work, we made use of a surfactant to prepare the nanofluid dispersion.

Commonly used surfactants in the preparation of nanofluids are sodium dodecyl sulfate (SDS)¹⁶⁻¹⁹, Gum Arabic¹⁷, sodium dodecylbenzene sulphonate (SDBS)¹⁸ and hexadecyltrimethylammonium bromide (CTAB)¹⁶. Sodium deoxycholate (DOC), a bile salt, commonly used for Density Gradient Ultracentrifugation experiments was used as the surfactant in the present study²⁴⁻²⁶. **The chemical structure of DOC is shown in Figure 3.** DOC possesses a rigid structure consisting of a cholesterol group with dissimilar sides²⁷. It consists of a steroid skeleton with a carboxylic acid side chain at one end and two hydroxyl groups on its steroid backbone. The two polar hydroxyl groups on the α -face and the methyl group on the β -face facilitate strong adsorption of DOC onto the surface of SWCNTs²⁷.

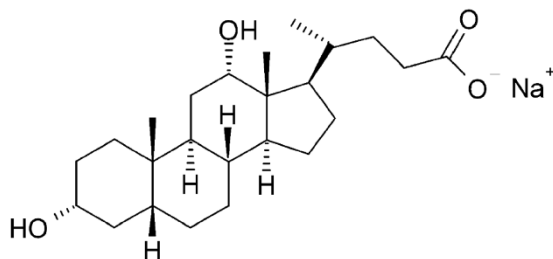


Figure 3: Chemical structure of Sodium deoxycholate ($C_{24}H_{39}NaO_4$)

Stable nanofluid dispersions were prepared by adding necessary loading of SWCNTs. For this purpose the SWCNT density was considered to be 1.6 g/cm^3 (assuming a SWCNT diameter of 1 nm and Van der Waals spacing of 0.34 nm). DOC loading of 0.75 w/v% was employed. The dispersions were subjected to bath sonication for 6 hours followed by tip sonication using an ultrasonic processor (Hielscher GmbH, UP-400S with H3/Micro Tip 3) for 2 hours at a power flux level of 368 W/cm^2 (80% amplification). Same sonication conditions are adopted for samples of different concentrations tested. Furthermore, it was also assumed that 5% of the mass is lost during the tip sonication and the losses are taken into account during the sample preparation. The pH of the SWCNT/water nanofluids was measured to be 7. The nanofluids remained highly stable, showing no visible signs of sedimentation even after 6 months of incubation.

2.4 Nanofluid characterization

DOC-encapsulated SWCNTs were further characterized using TEM (Hitachi H-9500) to see how the nanotubes are dispersed by the surfactant. TEM samples were prepared by performing dialysis for 24 hours to remove excess surfactant. Figure 4 shows the TEM image of DOC dispersed SWCNT.

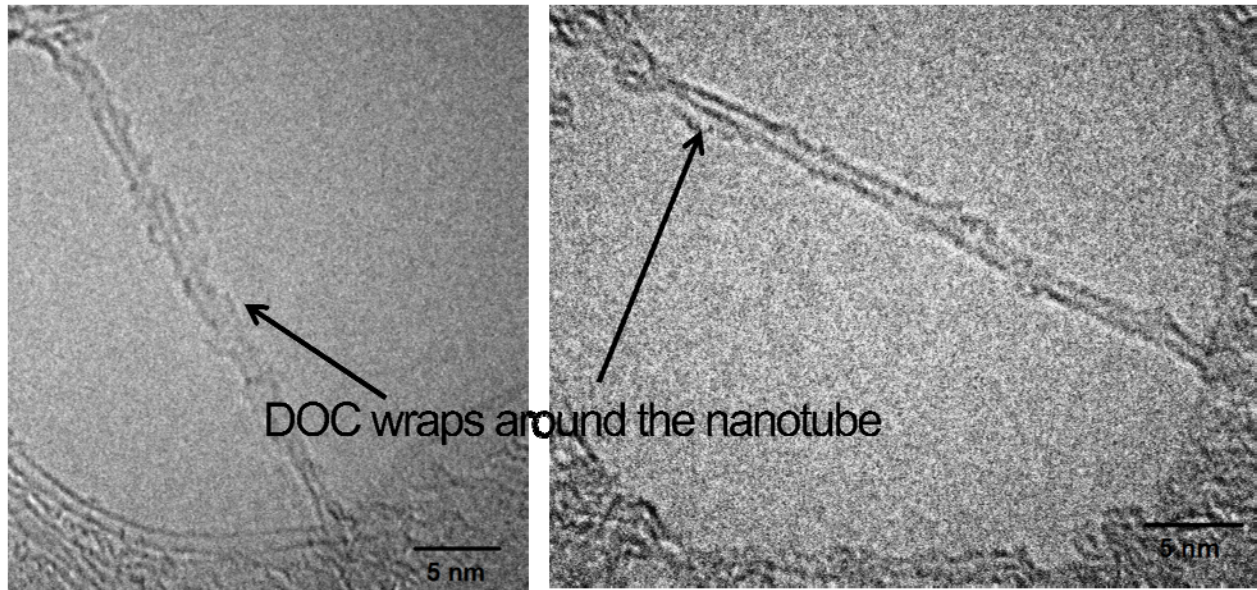


Figure 4: TEM visualization of surfactant-encapsulated SWCNTs. Image captured at an acceleration voltage of 200 kV.

Anionic surfactants like SDS form ellipsoidal or spherical micelles on the CNT surface. Unlike SDS, DOC having one hydrophilic side and one hydrophobic side wraps around the SWCNT instead of forming spherical or ellipsoidal micelles²⁷. The hydrophobic α -face contacts intimately with the side walls of the nanotube, while the hydrophilic β -face interfaces with water. The strong interaction between the hydrophobic side of DOC and the SWCNT sidewalls causes the surfactant to wrap around the SWCNT with a preferred orientation^{25,26}. TEM image shown in figure 4 support the mechanism of DOC wrapping reported in the literature²⁴⁻²⁶ based on Density Gradient Ultracentrifugation experiments.

DOC-dispersed SWCNTs were further characterized using optical absorption spectroscopy (OAS) and photoluminescence spectroscopy (PLE). The nanofluid dispersions were diluted to perform the measurements. Figure 5 shows a typical absorption spectrum obtained from SWCNTs dispersed in water using DOC. The absorbance spectrum shown in figure 5 consists of sharp peaks, which are characteristic of isolated nanotubes. The absorption peaks correspond to the first and second optical transitions (E_{11} and E_{22}) in semiconducting nanotubes and the first optical level of metallic nanotubes²⁸.

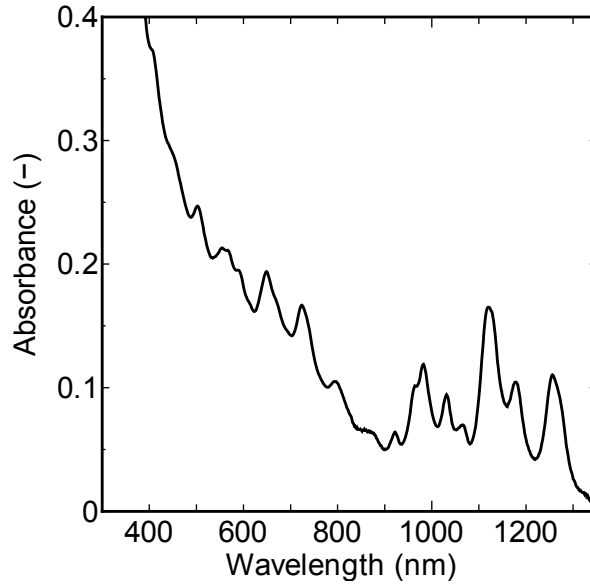


Figure 5: UV-Vis-NIR absorbance spectrum of SWCNTs dispersed in water using DOC.

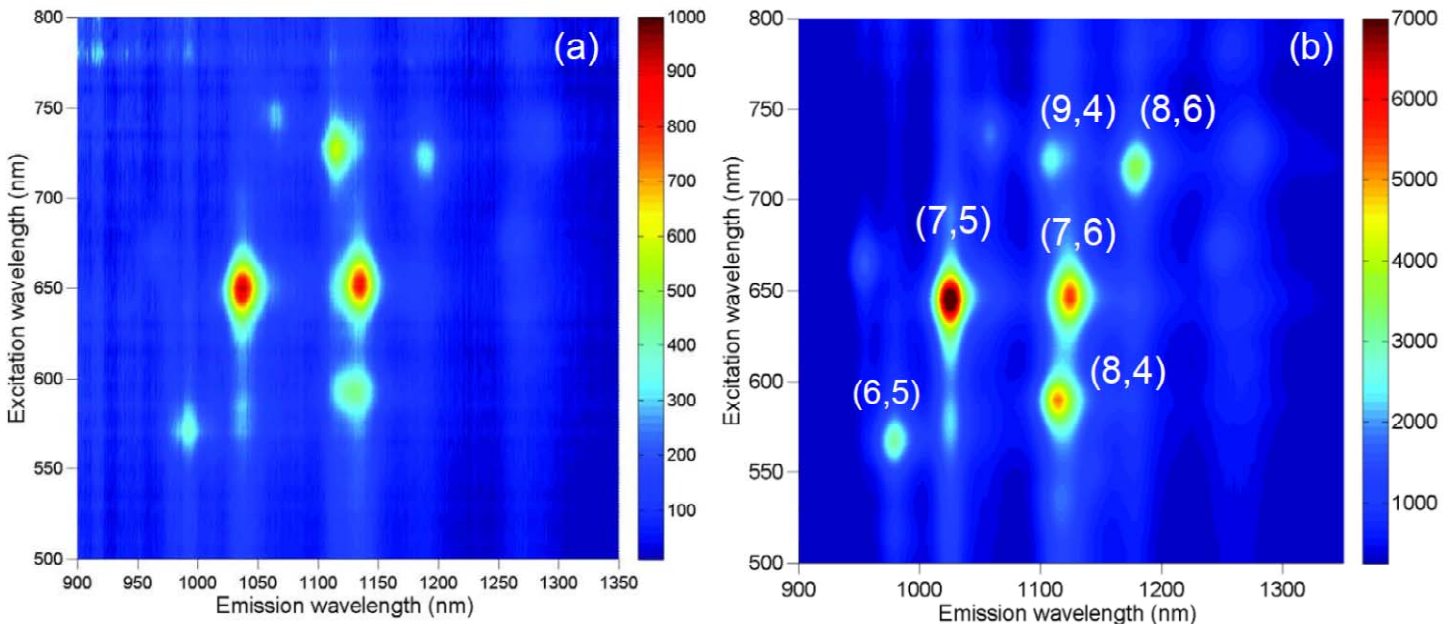


Figure 6: Photoluminescence excitation map of SWCNT/water nanofluid. Figure (6a) corresponds to the PLE map taken at 0.005 vol%. Figure 6(b) corresponds to the PLE map taken post centrifugation. Improved signal intensity due to the elimination of bundles is clearly evident in figure 6(b).

Figure 6 shows a PLE map of the dispersed SWCNTs with and without centrifugation. Figure 6a shows a PLE map of the suspension taken at a concentration of 0.005 vol%. The clear signals from various semiconducting SWCNTs demonstrate that a dispersion of well-isolated SWCNTs can be obtained even without centrifugation²⁹. A PLE map of the same sample after ultracentrifugation is shown in Fig. 6b. The signal is much more intense due to the removal of bundles, but no changes in spectral positions are evident after ultracentrifugation. This indicates that DOC is an effective surfactant for dispersing relatively high concentrations of SWCNTs, which can then be characterized using common spectroscopic techniques.

Atomic force microscopy (AFM) measurements (SII, SPI3800N) were performed in order to determine the mean length of the SWCNTs after sonication. The samples were prepared by dropping 10 μ L of the SWCNT dispersion on a silicon substrate and the substrate was heated at 333K for 30 minutes to evaporate the water. Figure 7(a) shows a typical AFM image of the DOC-wrapped SWCNTs. Figure 7(b) shows the SWCNTs length distribution predominantly ranging from 100 nm to 600 nm post sonication.

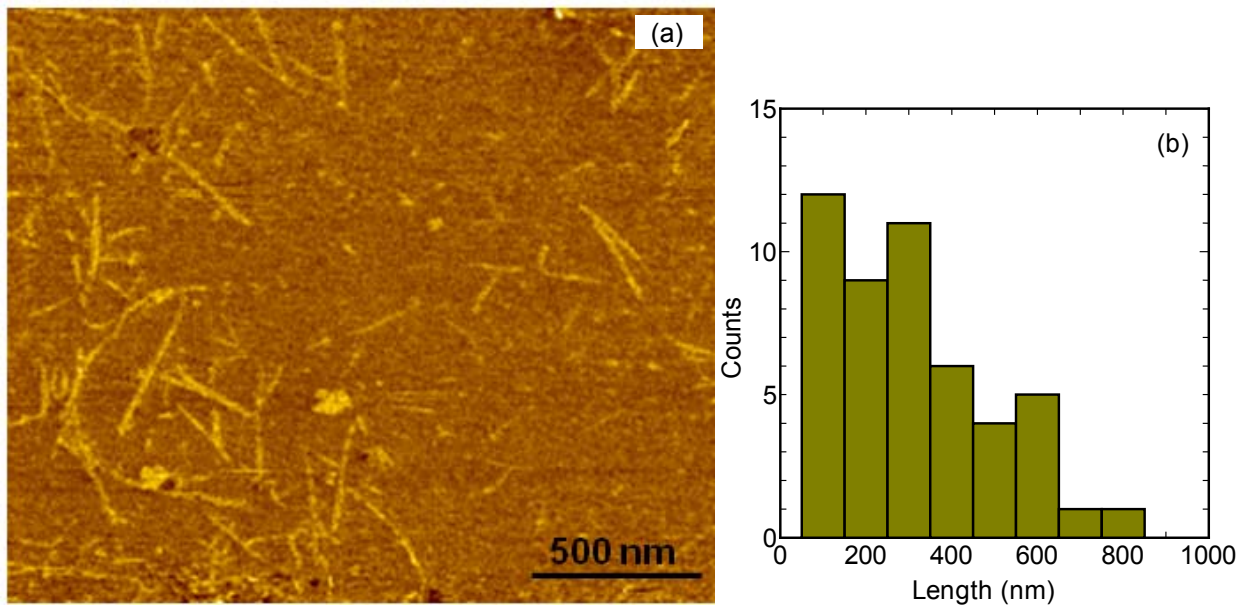


Figure 7: (a) AFM image of surfactant-encapsulated SWCNTs post sonication (SWCNT loading – 0.005 vol%). (b): Size wise length distribution of the SWCNTs.

2.5 Electrical conductivity measurement

The electrical conductivity of the SWCNT nanofluids was measured by pouring the dispersions into a specially prepared rectangular test cell made of plexiglass. The test cell consists of two parallel copper electrodes with an area A of 3 cm² separated by a distance L of 6.5 cm. The electrical conductivity ρ is calculated using the following equation, where R is the measured electrical resistance.

$$\rho = \frac{RA}{L} \quad (1)$$

2.6 Thermal conductivity measurement

To measure the thermal conductivity of electrically conducting nanofluids, we made use of the transient hot wire (THW) technique developed by Nagasaka and Nagashima³⁰. This technique is based on the measurement of the temporal response of the temperature of a hot wire when it is subjected to an electrical step input. We made use of a platinum (Pt) hot wire (diameter 76.4 μm) with an electrically insulating teflon coating (coating thickness 33.6 μm). The Pt wire acts as both the heater and an electrical resistance thermometer. During the experiments, the Pt wire is immersed in the test fluid and a step input is passed through it. The temperature rise of the hot wire is determined from the change in resistance of the hot wire, which is measured as a function of time using a Wheatstone-bridge circuit. With known electric power supply, the thermal conductivity is calculated from Fourier's law using the following equation.

$$k = \frac{Q}{4\pi L} \frac{d \ln t}{dT} \quad (2)$$

In equation (2), k is the thermal conductivity of the fluid, Q is the power supplied to the wire, L is the length of the hot wire, T is the temperature of the hot wire and t is time. The THW setup was calibrated using pure deionized water at different temperatures (see supporting information). For the thermal conductivity calculations, the data recorded between 0.2 and 1.9 s after the step input was used. Choosing the data in this

range eliminates effects associated with the thermal capacitance of the hot wire and the influence of natural convection. A detailed uncertainty analysis of the THW setup was carried out and the experimental uncertainty was found to be $\pm 2.5\%$.

3. Results and discussion

Electrical conductivity of the SWCNT/water nanofluid samples are plotted in figure 8. The Electrical conductivity increased sharply at very low SWCNT loading and then gradually saturated as the SWCNT loading increased, thus exhibiting clear percolation behaviour. Experimental data were fitted using a two-parameter equation $\rho = \rho_o(\phi - \phi_c)^t$ as per classical percolation theory³¹. Fitting the data using a power law equation shows a very low percolation threshold of $\phi_c = 0.0152$ vol% (0.025 wt%). The present results are comparable to the electrical percolation threshold of 0.024 wt% and 0.03 wt% reported for SWCNT/Poly (ethylene terephthalate)³² and SWCNT/Poly (ethylene oxide) composites³³.

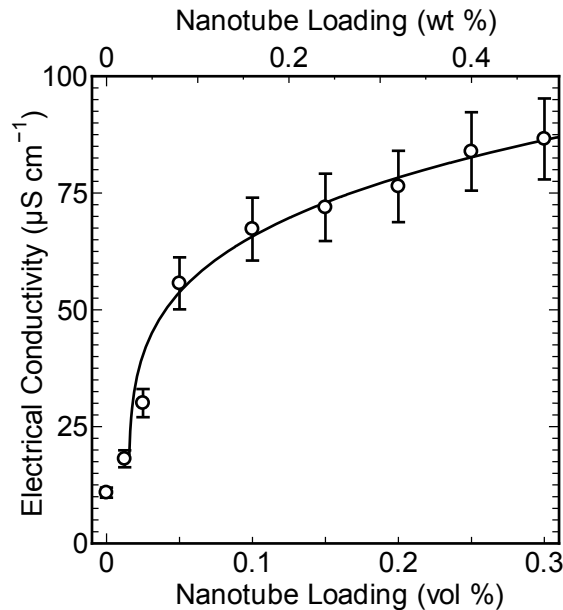


Figure 8: Electrical Conductivity of SWCNT/water nanofluids. A two-parameter fit as per classical percolation theory³¹ yielded a low percolation threshold of 0.0152 vol%.

Thermal conductivity of the SWCNT/water nanofluid samples was measured using the THW setup for different SWCNT loadings ranging from 0.1 to 0.3 vol%. Figure 9 shows the effective thermal conductivity versus different SWCNT loadings measured at room temperature. Thermal conductivity increased with increasing SWCNT loading in a linear fashion. This is clearly contradictory to the electrical conductivity behaviour as the electrical conductivity of the fluids showed a percolating behaviour while no obvious sign of percolation was noticed for thermal conductivity. Persistent heat conduction by water and low thermal conductivity contrast ratio (compared to electrical conductivity contrast ratio) between water/SWCNT does not result in a sharp increase in thermal conductivity at the percolation threshold³⁴.

In figure 9, we compare our thermal conductivity measurements for SWCNT/ethylene glycol (EG) nanofluids³⁵ with present experiments. SWCNT/EG nanofluids showed a higher thermal conductivity enhancement compared to that of the SWCNT/water nanofluids. Moreover, the SWCNT/EG effective thermal conductivity shows a non-linear increase with respect to SWCNT loading, whereas a linear increase is found in the case of the water based nanofluids. The number of contact points between the SWCNTs increase as a function of the square of the SWCNT loading, therefore one might associate the non-linear increase observed in SWCNT/EG nanofluids to the non-linear increase in the heat transport path³⁴. In our previous work, we pointed out that the stability of SWCNT/EG nanofluids was extremely poor, as the SWCNTs soon settled and formed larger aggregates. The non-linear tendency observed in the previous work was possibly due to the existence of larger aggregates. Efficient isolation of SWCNTs in water (compared to EG) may minimize the number of contact points thereby diminishing the heat transport path because resulting in a linear increase in effective thermal conductivity. Since the electrical conductivity measurements reveal a very low percolation threshold, it can be concluded that the SWCNTs forms a percolating network, which leads to better energy transport thereby

increasing the effective conductivity of the fluid. The thermal conductivity increase observed in the present experiments supports the mechanism of particle clustering in increasing the thermal conductivity of the fluid. **It needs to be pointed out the electrical conductivity and thermal conductivity increase remained almost the same for three months.**

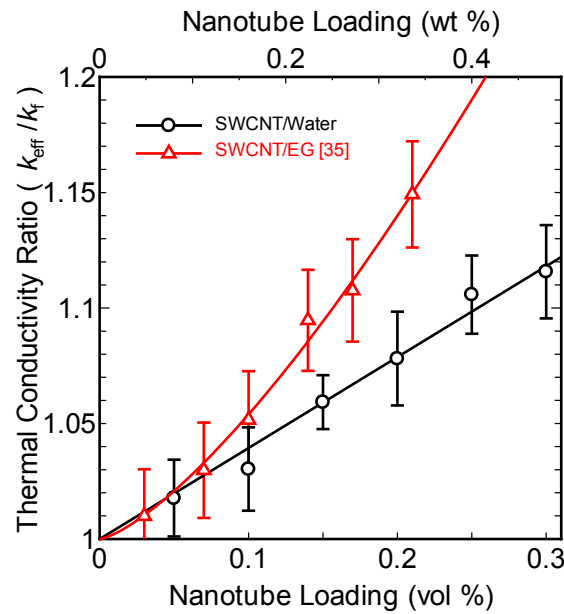


Figure 9: Thermal conductivity increase as a function of SWCNT loading in water

The effective thermal conductivity increase of the SWCNT/water nanofluid was also found to be temperature dependent. Figure 10 shows the effective thermal conductivity values for three volume concentrations at different temperatures. Figure 10 shows an additional 3-5% increase in effective thermal conductivity with increasing temperature. A maximum conductivity increase of 16% is obtained at a temperature of 333 K and a SWCNT loading of 0.3 vol%. Gharagozloo et al.³⁶ reported that nano particles tend to aggregate as time progresses, and correlated the temperature dependent increase observed to the increase in the size of the aggregates as a significant amount of time is often spent to heat the fluid during measurements. In order to examine this mechanism we performed a hysteresis measurement, which is shown in figure 11. **From figure 11, it is evident that the fluid effective thermal conductivity enhancement remains the same with respect to**

temperature irrespective of whether the fluid is heated or cooled (no hysteresis). This clearly rules out the possibility of “time-dependent aggregation”³⁶ as a probable mechanism for the temperature-dependent thermal conductivity increase.

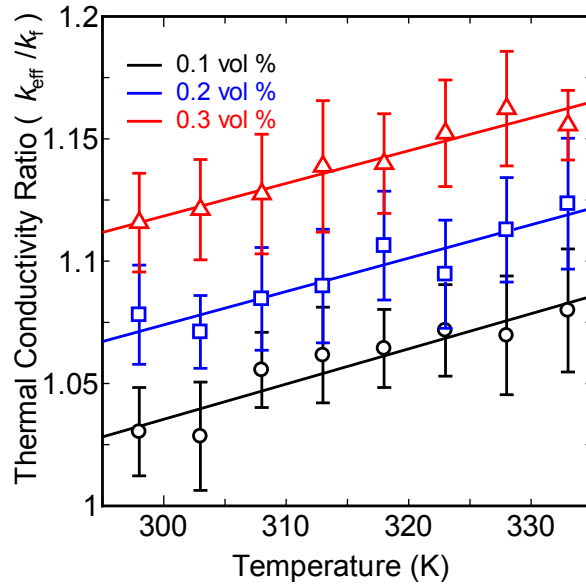


Figure 10: Thermal conductivity increase as a function of fluid temperature in water

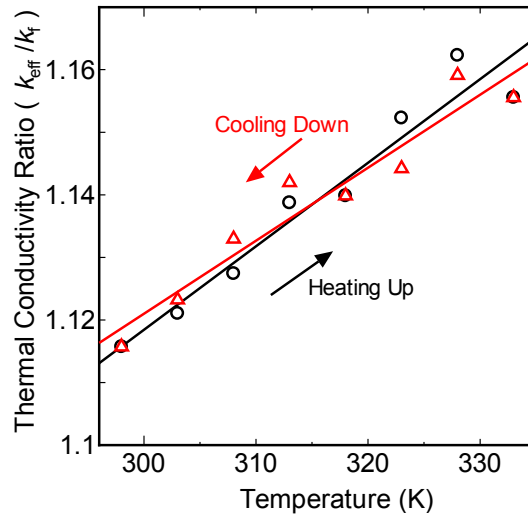


Figure 11: Comparison of thermal conductivity improvement during the heating and cooling process in water (SWCNT loading: 0.3 vol. %). The effective conductivity enhancement remains the same with respect to temperature irrespective of whether the fluid is heated or cooled.

Figure 12 shows a comparison of temperature-dependent thermal conductivity behaviour between the SWCNT/water and the SWCNT/EG based nanofluids. This figure shows that the SWCNT/EG nanofluids did not exhibit temperature dependent enhancement, while a different trend is observed in the case of SWCNT/water nanofluid.

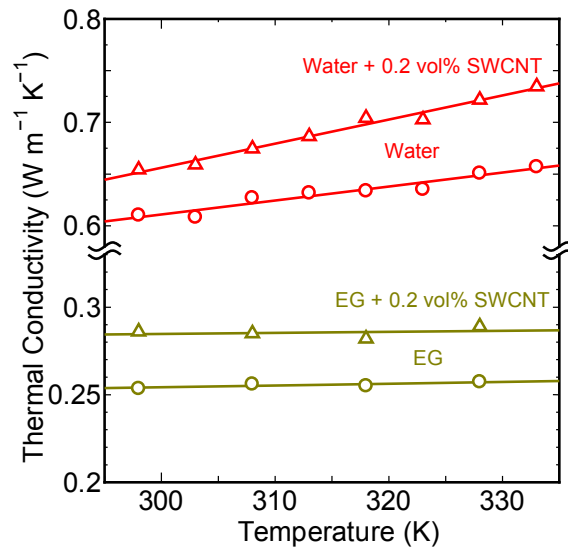


Figure 12: Temperature dependent thermal conductivity in SWCNT/water and SWCNT/EG nanofluids. Open circles correspond to base fluid measurements and open triangles correspond to SWCNT nanofluids

The difference in temperature dependent thermal conductivity variation could possibly indicate the critical role of Brownian motion in the fluid. Brownian motion depends on the fluid temperature and viscosity. Gupta and Kumar³⁷ suggested that the Brownian motion can enhance the thermal conductivity at higher temperatures up to 6%. Computational modeling of SWCNTs in water using random movement of Brownian thermal walkers, Duong et al.³⁸ reported temperature-based increase in thermal conductivity of water due to the enhanced diffusion of heat walkers. Tsyboulski et al.³⁹ experimentally found the translational diffusion coefficient of SWCNTs (D_{SWCNT}) in water range from 0.3 to 6 $\mu\text{m}^2/\text{s}$, which is much lower than the diffusion coefficient of

water ($D_w = 0.413 \text{ mm}^2/\text{s}$). However, the SWCNTs also exhibit rotational diffusion (D_r) which can be estimated using Broersma theory as follows⁴⁰:

$$D_r = \frac{3k_B T}{\pi\eta} \frac{\ln(L/d) - \gamma}{L^3} \quad (3)$$

In equation (3), L and d denote the length and diameter of the nanotube, respectively. k_B is the Boltzmann constant, T is the fluid temperature, η is the fluid viscosity and γ is the end correction coefficient (usually γ is assumed to be 0.8³⁹).

Equation (3) shows the rotational diffusion is inversely proportional to the cube length of the SWCNTs. A simple calculation assuming a SWCNT length of 250 nm and diameter of 1 nm gives a rotational diffusion of approximately 1000 s^{-1} . As the temperature is increased, the viscosity of the fluid reduces (from figure 13), which further improves the rotational diffusion of SWCNTs. Yunker et al.⁴¹ showed that short aspect ratio ellipsoids predominantly undergo rotational diffusion while large aspect ratio particles exhibited both mixed rotational and translational diffusion.

As previously discussed, the length distribution of SWCNTs in the present study is from 100 to 600 nm. It is thus possible to conclude that the high rotational diffusion induced by the presence of shorter SWCNTs lead to the temperature dependent increase in thermal conductivity. Since viscosity of EG is much higher (~35 times) than that of water, the influence of rotational diffusion is less pronounced in the SWCNT/EG nanofluid, thus does not cause any improvement in conductivity at higher temperature.

Figure 13 shows the comparison of viscosities of SWCNT/water nanofluids measured using a Cannon Fenske viscometer. Figure 13 shows that the viscosity of the nanofluids increased with increasing SWCNT concentration. The viscosity of the nanofluid decreased as the temperature increased, thus exhibiting similar behaviour of the base fluid. A viscosity increase of up to 30% was observed for SWCNT loading of 0.3 vol%. The increase in viscosity was approximately three times higher than the thermal conductivity enhancement

measured at room temperature. This strong increase in viscosity will have adverse effects in practical applications of such nanofluids.

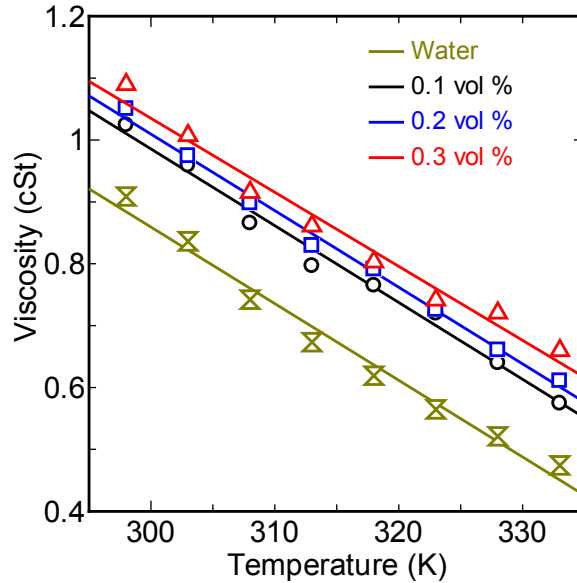


Figure 13: Viscosity of SWCNT/water nanofluids

Xie et al.¹⁵ reported an thermal conductivity increase of only 7% with 1 vol% MWCNT suspensions. Assael et al.¹⁶ reported an increase between 20% and 40% at 0.6 vol% of MWCNT loading at room temperature. Ding et al.¹⁷ reported a strong temperature dependent increase for aqueous suspensions consisting of MWCNTs. An increase of up to 80% was reported at a MWCNT loading of 1 wt% and at a temperature of 303 K. Baby and Ramaprabhu⁴² developed graphene-based nanofluids and reported an increment of up to 64% at a very low loading of 0.05 vol% at a temperature of 323 K and Nasiri et al.⁴³ recently reported the temperature dependent thermal conductivity increase of aqueous suspensions consisting of SWCNTs dispersed using SDS as the surfactant. An increase of up to 35% at a temperature of 323 K and a nanotube loading of 0.25 wt% was reported in their work. Similar temperature-dependent enhancement has also been reported by Glory et al.⁴⁴ for a water-based nanofluid. The present experimental thermal conductivity increase is marginally lower than the

previous reports. Proper characterization and systematic experiments, like the present case, need to be performed to minimize the discrepancy among experimental results from different research groups.

We also compared our experimental results with the effective medium theory (EMT)⁴⁵ and the Yamada–Ota model⁴⁶. Nan et al.⁴⁵ reported a model, for randomly embedded ellipsoidal particles embedded in a composite by incorporating the thermal boundary resistance (TBR) to estimate the effective thermal conductivity of the CNT based composites as follows:

$$\frac{k_{eff}}{k_b} = 1 + \frac{\phi L}{d} \frac{(k_p/k_b)}{\frac{L}{d} + \frac{2a_k}{d} \frac{k_p}{k_b}} \quad (4)$$

Here L and d are the nanotube length and diameter respectively. k_b is the base fluid thermal conductivity, k_p is the SWCNT thermal conductivity, k_{eff} is the effective fluid thermal conductivity, ϕ is SWCNT volume fraction, a_k is the Kapitza radius, which is defined as the product of thermal boundary resistance and the thermal conductivity of the base fluid ($a_k = TBR \times k_b$).

Zheng and Hong⁴⁷ reported a model by incorporating the TBR in the original Yamada–Ota model, and can be written as follows:

$$\frac{k_{eff}}{k_b} = \frac{(k_x/k_b) + \alpha - \alpha\phi[1 - (k_x/k_b)]}{(k_x/k_b) + \alpha + \phi[1 - (k_x/k_b)]} \quad (4)$$

where $k_x = \frac{k_p}{1 + \left(\frac{2k_p TBR}{L}\right)}$ and $\alpha = 2\phi^{0.2} \frac{L}{d}$. The notations in equation (4) are same as in equation (3). Note that

the TBR incorporated in the original Yamada–Ota model follows the same manner as reported by Nan et al⁴⁵. The original Yamada–Ota model was derived assuming a random orientation of the particles having a shape of parallelepiped neglecting the interparticle interactions and aggregation effects. For the present model

calculations, a fluid thermal conductivity of $0.598 \text{ W m}^{-1} \text{ K}^{-1}$ ⁴⁸, SWCNT thermal conductivity of $1750 \text{ Wm}^{-1}\text{K}^{-1}$ ⁸, aspect ratio of 350, and thermal boundary resistance (TBR) of $10^{-8} \text{ m}^2 \text{ K W}^{-1}$ ⁴⁹ were used.

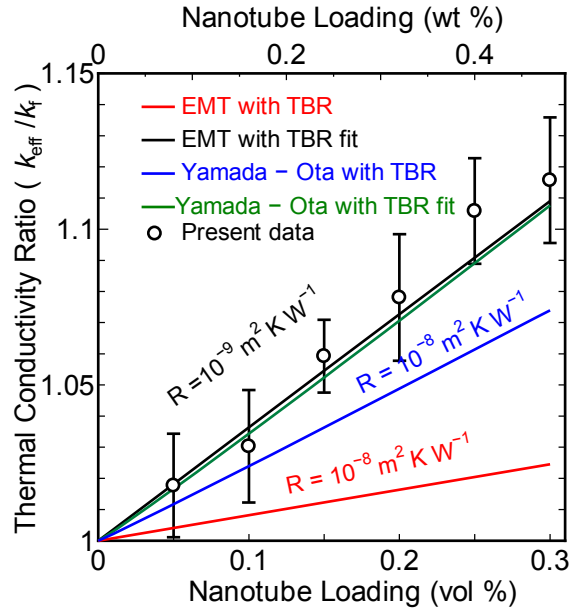


Figure 14: Comparison of experimental results with analytical models

Figure 14 shows the comparison of the model calculations with the present experimental results at room temperature. EMT theory predicts a less significant enhancement, while the modified Yamada–Ota model predicts an enhancement that is marginally less than the experimental results. Nevertheless, it can be understood from both models that the TBR plays a detrimental role in reducing the effective conductivity of the nanofluid, despite the high thermal conductivity of SWCNTs. By considering TBR as an unknown parameter and using the measured thermal conductivity increase, we estimated the interfacial resistance to be $2.8 \times 10^{-9} \text{ m}^2 \text{ K W}^{-1}$ and $6.8 \times 10^{-9} \text{ m}^2 \text{ K W}^{-1}$ based on fittings using the EMT and Yamada–Ota models, respectively. This corresponds to a thermal boundary conductance (inverse of TBR) of $300 \text{ MWm}^{-2} \text{ K}^{-1}$ (EMT fit) and $145 \text{ MW m}^{-2} \text{ K}^{-1}$ (Yamada–Ota fit) respectively. It is important to note that the estimated TBR value is one order of magnitude lower than the previous experimental report by Huxtable et al.⁴⁹ for SDS-encapsulated SWCNTs and simulations results of Maruyama et al.⁵⁰. Cherkasova and Shan⁵¹ reported TBR of similar order of magnitude for SDBS-encapsulated

MWCNTs in water. Marconnet et al.⁵² also reported a similar result for MWCNT-epoxy interfaces. We also found a TBR of similar order of magnitude in our experiments with SWCNT/EG suspensions³⁵. It needs to be noted that such a low TBR obtained from the EMT fit is clearly striking and contradicts the existing experimental and simulation results. The principal reason for this low TBR was that the EMT model does not take into account the effective length (percolated networks) and aggregation effects in the model.

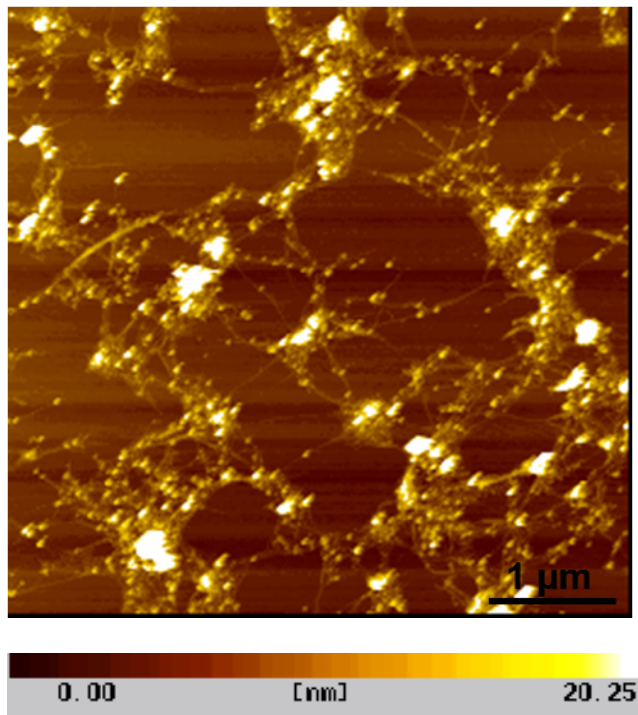


Figure 15: AFM visualization of 0.05 vol% SWCNTs. The presence of smaller aggregates and percolated networks to form a long heat transport path is clearly seen.

We performed AFM measurements at a higher concentration of 0.05 vol% SWCNT nanofluid to visualize the percolation behaviour and to calculate the effective length of SWCNTs in the actual suspension which is shown in figure 15. Figure 15 clearly shows the presence of small aggregates and connected networks having a percolation path of few micrometers. In figure 7, AFM image taken at very low concentration of 0.005 vol%, the SWCNTs seem to be highly isolated while in figure 15 such a feature is difficult to notice. Since figure 15

corresponds to a concentration much higher than the percolation threshold of 0.0152 vol% (based on electrical conductivity measurements), it is possible to conclude the SWCNTs are in connected networks, although the exact heat transport length is difficult to measure with our current experimental tools. When the thermal boundary resistance (TBR) is evaluated from equations 4 & 5 by using the mean aspect ratio as 350 (length 350 nm, diameter 1 nm) obtained from the measured thermal conductivity enhancement, we get an extremely low value. The low TBR resulting from this fitting is physically unreasonable and contradictory to the experimental and simulation results reported in references 49 and 50 respectively. Hence, to obtain a TBR which is consistent with the existing literature evidence, we estimate the effective percolation length as 2.5 μm (aspect ratio 2500) by fitting the experimental data again with the analytical models. By assuming a realistic effective heat transport length as 2.5 μm and repeating the TBR calculation yields a TBR of $2.1 \times 10^{-8} \text{ m}^2 \text{ K W}^{-1}$ and $4.9 \times 10^{-8} \text{ m}^2 \text{ K W}^{-1}$ for EMT and Yamada–Ota models, respectively. The present values are in good agreement with the existing experimental results.

It is evident from the present experimental results that the large TBR remains a hindrance in increasing the thermal conductivity of the fluid despite the high conductivity of SWCNTs. Based on MD simulations, Xu and Buehler⁵³ reported that the thermal boundary conductance for bare SWCNT-SWCNT junctions varies from 0.1 to 1 $\text{GWm}^{-2} \text{ K}^{-1}$, and infiltration of a polymer matrix will further improve the conductance by a maximum of 40%. Their simulations give an indication that by proper manipulation of TBR much higher thermal conductivity increase can be obtained in nanofluids as well as in nano composites. Besides, the authors also report that coating the CNT surface with metal layers like Au, Ni or Cu can further minimize TBR. This way of metal coating also has additional benefit that the metal layers also contribute to thermal conduction via electron transport⁵³. Both the methods are experimentally feasible techniques. However we believe functionalization with materials like polyethylene glycol (PEG) will be the right direction to minimize TBR as metal coating will

further increase the viscosity of the fluid. Such a way of PEG functionalized SWCNTs also have many medical applications⁵⁴.

4. Conclusions

Electrical conductivity, thermal conductivity and viscosity measurements were performed on SWCNT/water nanofluids in which the SWCNTs were dispersed using sodium deoxycholate surfactant. Electrical conductivity measurements revealed a sharp increase in electrical conductivity near the percolating threshold, while no such behaviour was noticed for thermal conductivity. Effective thermal conductivity of the nanofluids showed an additional 3-5% increase in conductivity with increasing temperature. Viscosity of the SWCNT nanofluids increased with increasing SWCNT concentration and showed a threefold increase compared to the thermal conductivity enhancement. The experimental results were compared with Nan's effective medium theory and the Yamada–Ota model, the latter of which performed better than effective medium theory and was in good agreement with the experimental data. The critical role of thermal boundary resistance—which limits the effective thermal conductivity improvement—was discussed, and possible ways to minimize the thermal boundary resistance was recommended as a scope for future research.

Acknowledgments

This work was financially supported in part by Grant-in-Aid for Scientific Research (22226006 and 19054003), the Japanese Government Monbukagakusho (MEXT) Scholarship, and the “Global Center of Excellence for Mechanical Systems Innovation” (GMSI). A part of this work was conducted in the Research Hub for Advanced Nano Characterization, The University of Tokyo, supported by the Ministry of Education, Culture, Sports, Science and Technology, Japan.

References

- [1] J. Fan, L. Wang; Review of Heat Conduction in Nanofluids; *J. Heat Transfer* 133, 040801 (2011).

- [2] W. Daungthongsuk, S. Wongwises; A critical review of convective heat transfer of nanofluids; *Renew. Sustain. Energy Rev.* 11, 797 (2007).
- [3] C. Kleinstreuer, Y. Feng; Experimental and theoretical studies of nanofluid thermal conductivity enhancement: a review; *Nanoscale Res. Lett.* 6, 229 (2011).
- [4] L. Godson, B. Raja, D.M. Lal, S. Wongwises; Enhancement of heat transfer using nanofluids-An overview; *Renew. Sustain. Energy Rev.* 14, 629 (2010).
- [5] J.A. Eastman, S.U.S. Choi, S. Li, W. Yu, L. J. Thompson; Anomalously increased effective thermal conductivities of ethylene glycol-based nanofluids containing copper nanoparticles; *Appl. Phys. Lett.* 78, 718 (2001).
- [6] J. Buongiorno, D.C. Venerus, N. Prabhat, T. McKrell, J. Townsend, R. Christianson et al; A benchmark study on the thermal conductivity of nanofluids; *J. Appl. Phys.* 106, 094312 (2009).
- [7] S.U.S. Choi, Z.G. Zhang, W. Yu, F.E. Lockwood, E.A. Grulke; Anomalous thermal conductivity enhancement in nanotube suspensions; *Appl. Phys. Lett.* 79, 2252 (2001).
- [8] J. Hone, M. Whitney, A. Zettl; Thermal conductivity of single-walled carbon nanotubes; *Phys. Rev. B* 59, 2514 (1999).
- [9] P. Kim, L. Shi, A. Majumdar, P.L. McEuen; Thermal transport measurements of individual multiwalled nanotubes; *Phys. Rev. Lett.* 87, 215502-1 (2001).
- [10] C.H. Yu, L. Shi, Z. Yao, D.Y. Li, A. Majumdar; Thermal conductance and thermopower of an individual single-wall carbon nanotube; *Nano Lett.* 5, 1842 (2005).
- [11] E. Pop, D. Mann, Q. Wang, K. Goodson, H.J. Dai; Thermal conductance of an individual single-wall carbon nanotube above room temperature; *Nano Lett.* 6, 96 (2006).
- [12] T.Y. Choi, D. Poulikakos, J. Tharian, U. Sennhauser; Measurement of the thermal conductivity of individual carbon nanotubes by the four-point three-omega method; *Nano Lett.* 6, 1589 (2006).

- [13] S. Berber, Y.K. Kwon, D. Tománek; Unusually high thermal conductivity of carbon nanotubes; *Phys. Rev. Lett.* 84, 4613 (2000).
- [14] S. Maruyama; A molecular dynamics simulation of heat conduction of a finite length single-walled carbon nanotube; *Microscale Therm. Eng.* 7, 41 (2003).
- [15] H.Q. Xie, H. Lee, W. Youn, M. Choi; Nanofluids containing multiwalled carbon nanotubes and their enhanced thermal conductivities; *J. Appl. Phys.* 94, 4967 (2003).
- [16] M.J. Assael, I.N. Metaxa, J. Arvanitidis, D. Christofilos, C. Lioutas; Thermal conductivity enhancement in aqueous suspensions of carbon multi-walled and double-walled nanotubes in the presence of two different dispersants; *Int. J. Thermophys.* 26, 647 (2005).
- [17] Y.L. Ding, H. Alias, D.S. Wen, R.A. Williams; Heat transfer of aqueous suspensions of carbon nanotubes (CNT nanofluids); *Int. J. Heat Mass Transfer* 49, 240 (2006).
- [18] D.S. Wen, Y.L. Ding; Effective thermal conductivity of aqueous suspensions of carbon nanotubes (carbon nanotubes nanofluids); *J. Thermophys. Heat Transfer* 18, 481 (2004).
- [19] P. Garg, J.L. Alvarado, C. Marsh, T.A. Carlson, D.A. Kessler, K. Annamalai; An experimental study on the effect of ultrasonication on viscosity and heat transfer performance of multi-wall carbon nanotube-based aqueous nanofluids; *Int. J. Heat Mass Transfer* 52, 5090 (2009).
- [20] M.S. Liu, M.C.C. Lin, I.T. Huang, C.C. Wang; Enhancement of thermal conductivity with carbon nanotube for nanofluids; *Int. Comm. Heat Mass Transfer* 32, 1202 (2005).
- [21] S. Maruyama, R. Kojima, Y. Miyauchi, S. Chiashi, M. Kohno; Low-temperature synthesis of high-purity single-walled carbon nanotubes from alcohol; *Chem. Phys. Lett.* 360, 229 (2002).
- [22] R. Saito, G. Dresselhaus, M.S. Dresselhaus; Trigonal warping effect of carbon nanotubes; *Phys. Rev. B* 61, 2981 (2000).

- [23] P. Araujo, S. Doorn, S. Kilina, S. Tretiak, E. Einarsson, S. Maruyama et al; Third and fourth optical transitions in semiconducting carbon nanotubes; *Phys. Rev. Lett.* 98, 067401 (2007).
- [24] F. Bonaccorso, T. Hasan, P. H. Tan, C. Sciascia, G. Privitera, G. Di Marco, P. G. Gucciardi, A. C. Ferrari; Density Gradient Ultracentrifugation of Nanotubes: Interplay of Bundling and surfactant encapsulation; *J. Phys. Chem. C* 114, 1105 (2010).
- [25] P. Zhao, E. Einarsson, R. Xiang, Y. Murakami, S. Maruyama; Controllable Expansion of Single-Walled Carbon Nanotube Dispersions Using Density Gradient Ultracentrifugation; *J. Phys. Chem. C* 114, 3064 (2010).
- [26] P. Zhao, E. Einarsson, G. Lagoudas, J. Shiomi, S. Chiashi, S. Maruyama; Tunable separation of single walled carbon nanotubes by dual surfactant Density Gradient Ultracentrifugation; *Nano Res.* 4, 623 (2011).
- [27] N.A. Mazer, M.C. Carey, R.F. Kwasnick, G.B. Benedek; Quasielastic light scattering studies of aqueous biliary lipid systems. Size, shape, and thermodynamics of bile salt micelles; *Biochem.* 18, 4831 (1979).
- [28] A. Hagen, T. Hertel; Quantitative analysis of optical spectra from individual single-wall carbon nanotubes; *Nano Lett.* 3, 383 (2003).
- [29] S. M. Bachilo, M.S. Strano, C. Kittrell, R.H. Hauge, R.E. Smalley, R.B. Weisman; Structure assigned optical spectra of single walled carbon nanotubes; *Science* 298, 075403 (2002).
- [30] Y. Nagasaka, A. Nagashima; Absolute Measurement of the Thermal-Conductivity of Electrically Conducting Liquids by the Transient Hot-Wire Method; *J. Phys. E Sci. Instrum.* 14, 1435 (1981).
- [31] D. Stauffer, A. Aharony; Introduction to percolation theory, 2nd ed. London: Taylor & Francis; (1994).
- [32] J.J. Hernández, M.C. García Gutiérrez, A. Nogales, D.R. Rueda, M. Kwiatkowska, Szymczyk et al; Influence of preparation procedure on the conductivity and transparency of SWCNT-polymer nanocomposites; *Comp. Sci. Tech.* 69, 1867 (2009).
- [33] T. Chatterjee, K. Yurekli, G. Hadjiev, R. Krishnamoorti; Single walled carbon nanotube dispersions in Poly (ethylene oxide); *Adv. Func. Mater.* 15, 1832 (2005).

- [34] N. Shenogina, S. Shenogin, L. Xue, P. Keblinski; On the lack of thermal percolation in carbon nanotube composites; *Appl. Phys. Lett.* 87, 133106-1 (2005).
- [35] S. Harish, K. Ishikawa, E. Einarsson, S. Aikawa, S. Chiashi, J. Shiomi, S. Maruyama; Enhanced thermal conductivity of ethylene glycol with single walled carbon nanotube inclusions. *Int. J. Heat Mass Transfer* 55, 3885 (2012).
- [36] P.E.Gharagozloo, K.E. Goodson; Aggregate fractal dimensions and thermal conductance in nanofluids; *J. Appl. Phys.* 108, 074309 (2010).
- [37] A. Gupta, R. Kumar; Role of Brownian motion on the thermal conductivity enhancement of nanofluids; *Appl. Phys. Lett.* 91, 223102 (2007).
- [38] H.M.Duong, D.V.Papavassiliou, K.J.Mullen, B.L.Wardle, S. Maruyama; Calculated Thermal Properties of Single-Walled Carbon Nanotube Suspensions; *J. Phys. Chem. C* 112, 19860 (2008).
- [39] D.A. Tsyboulski, S.M. Bachilo, A.B. Kolomeisky, R. Bruce Weisman; Translational and rotational dynamics of individual single walled carbon nanotubes in aqueous suspension; *ACS Nano* 2, 1770 (2008).
- [40] S. Broersma; Rotational diffusion constant of a cylindrical particle; *J. Chem. Phys.* 32, 1626 (1960).
- [41] P. Yunker, K. Chen, Z. Zhang, W. Ellenbroek, A. Liu, A.Yodh; Rotational and translational phonon modes in glasses composed of ellipsoidal particles; *Phys. Rev. E* 83, 011403 (2011).
- [42] T.T. Baby, S. Ramaprabhua; Investigation of thermal and electrical conductivity of graphene based nanofluids; *J. Appl. Phys.* 108, 124308 (2010).
- [43] A. Nasiri, M. Shariaty-Niasar, A.M. Rashidi, R. Khodafarin; Effect of CNT structures on thermal conductivity and stability of nanofluid; *Int. J. Heat Mass Transfer* 55, 1529 (2012).
- [44] J. Glory, M. Bonetti, M. Helezen, M. Mayne-L'Hermite, C. Reynaud; Thermal and electrical conductivities of water-based nanofluids prepared with long multiwalled carbon nanotubes; *J. Appl. Phys.* 103, 094309 (2008).

- [45] C.W.Nan, R. Birringer, D.R. Clarke, H. Gleiter; Effective thermal conductivity of particulate composites with interfacial thermal resistance; *J. Appl. Phys.* 81, 6692 (1997).
- [46] E. Yamada, T. Ota; Effective thermal conductivity of dispersed materials; *Heat Mass Transfer* 13, 27 (1980).
- [47] Y. Zheng, H. Hong; Modified model for effective thermal conductivity of nanofluids containing carbon nnaotubes; *J. Thermophys. Heat Transfer* 21, 658 (2007).
- [48] American Society of Testing and Materials; Standard test method for thermal conductivity of liquids; ASTM D2717 (2009).
- [49] S.T. Huxtable, D.G. Cahill, S. Shenogin, L.P. Xue, R. Ozisik, P. Barone et al; Interfacial heat flow in carbon nanotube suspensions; *Nat. Mater.* 2, 731 (2003).
- [50] S. Maruyama, Y. Igarashi, Y. Taniguchi, J. Shiomi; Anisotropic heat transfer of single walled carbon nanotubes; *J. Therm Sci Tech.* 1, 138 (2006).
- [51] A.S. Cherkasova, J.W.Shan; Particle Aspect-Ratio and Agglomeration-State Effects on the Effective Thermal Conductivity of Aqueous Suspensions of Multiwalled Carbon Nanotubes; *J. Heat Transfer* 132, 082402 (2010).
- [52] A.M. Marconnett, N.Yamamoto, M.A. Panzer, B.L.Wardle, K.E. Goodson; Thermal Conduction in Aligned Carbon Nanotube-Polymer Nanocomposites with High Packing Density; *ACS Nano* 5, 4818 (2011).
- [53] Z. Xu, M.J. Buehler; Nanoengineering heat transfer performance at carbon nanotube interfaces; *ACS Nano* 3, 2767 (2009).
- [54] M. Shim, N. W.S. Kam, R.J. Chen,Y. Li, H. Dai; Functionalization of carbon nanotubes for biocompatibility and biomolecular recognition; *Nano Lett.* 2, 285 (2002).

Supporting Information

Temperature dependent thermal conductivity increase of aqueous nanofluid with single walled carbon nanotube inclusions

Sivasankaran Harish¹, Kei Ishikawa¹, Erik Einarsson^{1,2}, Shinya Aikawa¹, Taiki Inoue¹,

Pei Zhao¹, Makoto Watanabe¹, Shohei Chiashi¹, Junichiro Shiomi¹, Shigeo Maruyama^{1*}

¹Department of Mechanical Engineering, The University of Tokyo, 7-3-1 Hongo, Bunkyo-ku, Tokyo 113-8656,
Japan

²Global Center of Excellence for Mechanical Systems Innovation, The University of Tokyo,
7-3-1 Hongo, Bunkyo-ku, Tokyo 113-8656, Japan

Theoretical Formulation

The transient temperature response T at a distance r from an ideal infinite line source is written in the form¹:

$$T = \frac{q}{4\pi\alpha} \int_{r^2/4\alpha t}^{\infty} \frac{e^{-a}}{a} da \quad (1)$$

Where q is the heat flux per unit length, α is the thermal diffusivity of the fluid and t is the time. The solution of the equation (1) is shown in figure 1. Equation (1) is plotted for varying time assuming a heat flux of 2 Wm^{-1} and the thermal diffusivity of fluid as $0.143 \text{ mm}^2 \text{ s}^{-1}$. For $t > 0$, the temperature continuously increases in the infinite medium as shown in figure 1. The temperature was maximum at the ideal heat source (zero radius) and decays exponentially with increasing radius r .

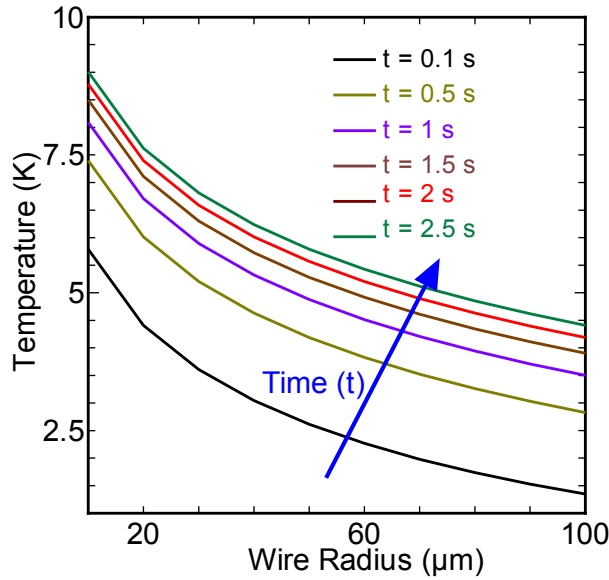


Figure 1: Solution of equation (1)

Nagasaka and Nagashima² derived the analytical solution for an electrically insulated wire to measure the thermal conductivity (K) of surrounding fluid. The solution takes the form as follows:

$$\Delta T = \frac{q}{4\pi K} \left(\ln t + A + \frac{1}{t} (B \ln t + C) \right) \quad (2)$$

In equation (2) A , B and C are constants determined by the geometry of the wire, thermal diffusivity of the fluid, insulation coating, material of the hot wire and the thermal conductivity of the insulation layer. When the $1/t$ term in the equation (2) is small, the constant term A shifts the ΔT term without changing the slope of the equation 2. Thus, the thermal conductivity of the fluid can be calculated using the simplified expression as follows:

$$K = \frac{q}{4\pi} \left(\frac{d \ln t}{dT} \right) \quad (3)$$

Error associated with the finite length of the wire is calculated using the expression prescribed by Healey et al³.

The expression is written in the form as follows:

$$\frac{dT}{d \ln t} = \frac{q}{4\pi K} (1 - \delta) \quad (4)$$

Where δ is the error associated with the finite length of the wire. The error δ is calculated using the expression as follows:

$$\delta = -\frac{e^{-L^2/16\alpha t}}{\pi} \left\{ \frac{\sqrt{16\alpha t}}{L} + \frac{L}{r} \left[\frac{K_w}{K} - \frac{(\rho C_p)_w}{\rho C_p} \right] \frac{\ln(4\alpha t/r^2 K)}{(4\alpha t/r^2 K)^{3/2}} \right\} \quad (5)$$

In equation 5, the subscript w denotes the properties of the hot wire. For the present system of the hot wire diameter ($2r$) 76.4 μm and length (L) 0.025 m, the error is calculated to be of the magnitude 10^{-4} .

When using equation (3) to calculate the thermal conductivity, it is necessary to know the starting time and the ending time to compute the slope. Healey et al. [3] also suggested the initial time to be between 10 ms $< t < 100$ ms. However, the ending time depends on the system design and varies between every setup. For the present system, we found that beyond 2s natural convection effect sets in. Figure 2 shows a raw data profile obtained from our experiment is shown. Figure 3 shows the $\ln t$ versus the temperature rise plot. The linear region in figure 3 is fitted using a least squares fit to compute the slope.

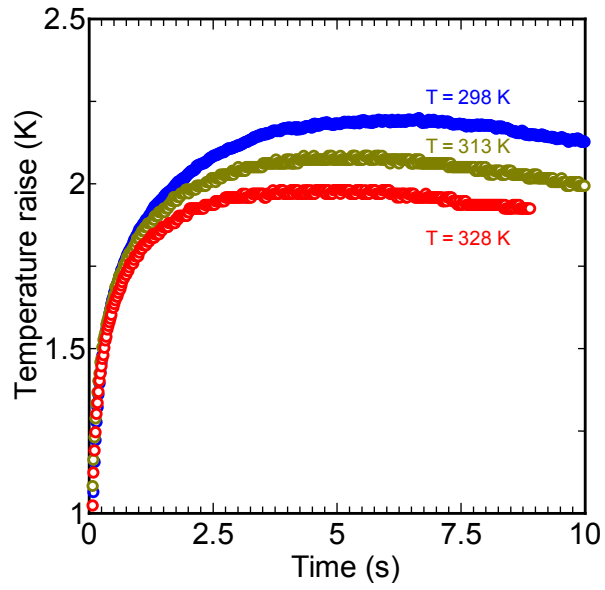


Figure 2: Temperature raise as a function of time

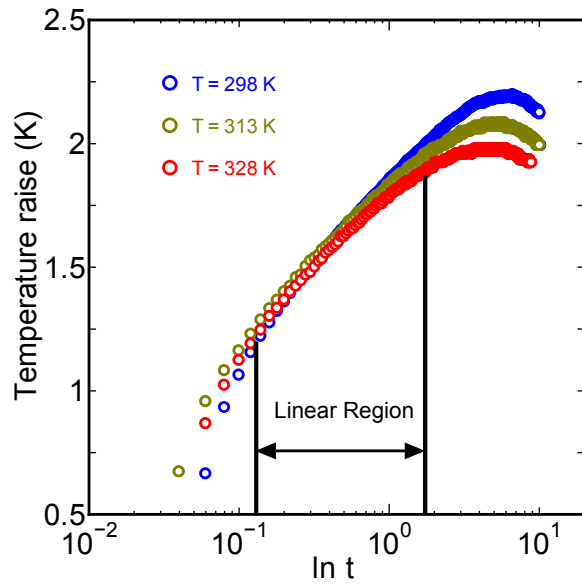


Figure 3: Logarithm of time Vs Temperature rise

Reference

[1] H.S. Carslaw, J.C. Jaeger; Conduction of Heat in Solids, 2nd ed USA: Oxford University Press; (1986).

- [2] Y. Nagasaka, A. Nagashima; Absolute Measurement of the Thermal-Conductivity of Electrically Conducting Liquids by the Transient Hot-Wire Method; *J. Phys. E Sci. Instrum.* 14,12 (1981).
- [3] J.J. Healy, J.J. De Groot, J. Kestin; The theory of the transient hot wire method for measuring thermal conductivity; *Physica.* 82C (1976).